

Article

Power Generation from Concentration Gradient by Reverse Electrodialysis in Dense Silica Membranes for Microfluidic and Nanofluidic Systems

Sang Woo Lee, Hyun Jung Kim and Dong-Kwon Kim *

Received: 28 October 2015; Accepted: 12 January 2016; Published: 15 January 2016
Academic Editor: Ling Bing Kong

Department of Mechanical Engineering, Ajou University, Suwon 443-749, Korea;
sadf21@ajou.ac.kr (S.W.L.); hyunkim@ajou.ac.kr (H.J.K.)

* Correspondence: dkim@ajou.ac.kr; Tel.: +82-31-219-3660; Fax: +82-31-219-1611

Abstract: In this study, we investigate power generation by reverse electrodialysis in a dense silica membrane that is between two NaCl solutions with various combinations of concentrations. Each silica membrane is fabricated by depositing a silica layer on a porous alumina substrate via chemical vapor deposition. The measured potential-current (V - I) characteristics of the silica membrane are used to obtain the transference number, diffusion potential, and electrical resistance. We develop empirical correlations for the transference number and the area-specific resistance, and present the results of power generation by reverse electrodialysis using the fabricated silica membranes. The highest measured power density is 0.98 mW/m^2 . In addition, we develop a contour map of the power density as a function of NaCl concentrations on the basis of the empirical correlations. The contour map shows that a power output density of 1.2 mW/m^2 is achievable with the use of silica membranes and is sufficient to drive nanofluidic and microfluidic systems. The dense silica membrane has the potential for use in micro power generators in nanofluidic and microfluidic systems.

Keywords: power generation; reverse electrodialysis; silica membrane; concentration gradient

1. Introduction

Energy sources are increasingly important for nanofluidic and microfluidic systems that are used in applications such as environmental monitoring with wireless sensor networks and implantable medical devices [1]. Therefore, considerable effort over several decades has been devoted to the investigation of energy conversion devices for nanofluidic and microfluidic systems [2,3]. These devices were developed not only by miniaturization and improvement of conventional energy conversion machines, but also by the application of truly novel methods of energy conversion [2]. Miniaturized conventional devices include miniaturized heat engines, micro fuel cells, microreactors, miniaturized gas turbines, and microbatteries. Whalen *et al.* [4] developed a micro heat engine in which a piezoelectric membrane extracts power from two-phase working fluids. Chohan *et al.* [5] presented a microfluidic fuel cell that utilizes the occurrence of microscale multistream laminar flow to keep the fuel and oxidant streams separated but in diffusional contact. On the other hand, novel methods to convert energy using microscale fabrication include generation of streaming potential through a nanochannel and biologically inspired methods. Van der Heyden *et al.* [6] investigated power generation by a streaming potential produced by pressure-driven transport of ions in nanochannels. Tanaka *et al.* [7] developed a microspherical heart-like pump, which can convert chemical energy flowing into cells to mechanical energy of a fluid stream. Chang and Yang [8] derived an exact expression for the figure of merit to calculate the electrokinetic energy conversion efficiency and power of an ion-selective nanopore. They found that the highest efficiency for a

non-slip cation-selective nanopore is 9.7%. They also theoretically and numerically investigated the electrokinetic energy conversion in short-length nanofluidic channels, taking into account reservoir resistance and concentration polarization effects [9]. These studies focused on conversion from hydrodynamic, chemical, and thermal energy to electrical energy.

The Gibbs free energy of mixing can be converted to electrical energy for nanofluidic and microfluidic systems using inorganic membranes. According to reference [10], inorganic membranes can be divided into two structural categories, dense and porous inorganic membranes, which can have a significant impact on their performance as separators. Dense membranes are free of discrete, well-defined pores or voids, as shown in Figure 1a. In contrast, porous membranes show well-defined straight or tortuous pores across the membrane thickness, as shown in Figure 1b. In the porous inorganic membrane, an aqueous solution fills the nanopores throughout the membrane, and surface ionization, ion adsorption, and ion dissolution cause the surface of the nanopores to become charged [11]. These surface charges draw counter ions toward the surface and repel co-ions (Figure 1a). On the other hand, the dense inorganic membrane consists of an irregular atomic network with fixed anionic or cationic groups [12]. These groups have an affinity for counter ions that can be adsorbed at ionic sites within the membrane [13]. When an electrolyte concentration gradient is applied to either type of membrane, counter ions are transported through the layer much more easily than co-ions, resulting in a net charge migration of ions (Figure 1b) [14]. Therefore, the Gibbs free energy of mixing, which forces ion diffusion, can be converted into electrical energy. This energy conversion process is called reverse electro dialysis.

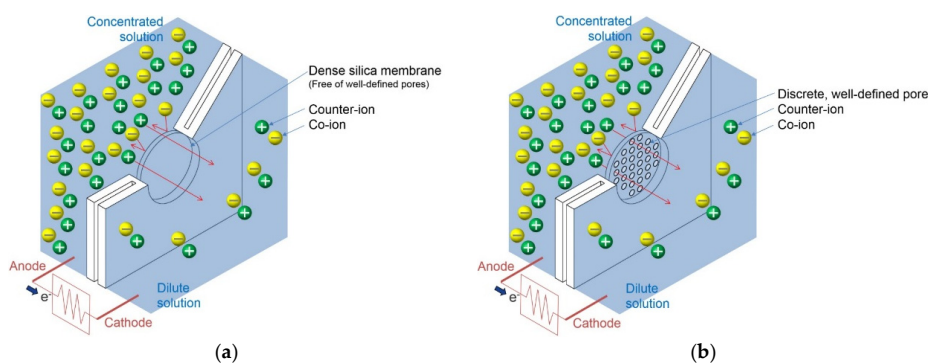


Figure 1. Power generation from concentration gradient by reverse electro dialysis: (a) in a dense silica membrane; and (b) in a porous membrane.

Recently, nanopores and nanofluidic channels have been widely investigated as porous inorganic membranes for use in reverse electro dialysis. Kim *et al.* [15] showed that silica nanochannels, fabricated by a standard semiconductor manufacturing process, can harvest energy by reverse electro dialysis. They experimentally investigated the power generated by 4 nm, 26 nm, and 80 nm high nanochannels that were between two KCl solutions with various combinations of concentrations. The highest power output measured was 2.89 pW. Ouyang *et al.* [16] conducted a proof-of-concept experiment using a nanofluidic crystal of packed silica nanoparticles. They achieved a power output of 1.18 nW with their prototype cell. Kim *et al.* [17] investigated the potential of alumina nanopores for reverse electro dialysis. Yeh *et al.* [18] performed numerical simulations based on the full Poisson–Nernst–Planck (PNP) equations to investigate reverse electro dialysis in negatively charged conical nanopores, and showed the maximum power conversion efficiency reaches 45%. On the other hand, reverse electro dialysis in dense inorganic membranes has not been investigated yet. These membranes are suitable for use in micro power generators and microbatteries where they can generate power more reliably because they do not shrink and swell in response to their environment [19]. In addition, the performance of dense membranes is not as affected by biofouling as porous membranes [20]. In particular, because dense silica membrane can be fabricated by the standard complementary metal-oxide-semiconductor

(CMOS) process, it has the potential for use in nanofluidic and microfluidic devices. This led us to investigate the potential of dense silica membrane for the use in reverse electro dialysis systems. We can expect that a dense silica membrane can be used for reverse electro dialysis, because the ion-selective properties of glass/electrolyte interfaces were recognized early in the 20th century, and glass electrodes have been used since then for measurements of pH and the activities of alkali ions [21]. However, the maximum power densities that can be achieved using a dense silica membrane, and the conditions under which these densities are achieved, are unclear. This lack of clarity is due to the fact that, to the best of our knowledge, there have been no previous studies focused on power generation by reverse electro dialysis in a dense silica membrane located between two solutions having different concentrations.

In this study, we investigated power generation using dense silica membranes by placing a silica membrane between two NaCl solutions with various combinations of concentrations. The silica membrane was fabricated by depositing a silica layer on a porous alumina substrate via chemical vapor deposition. We measured the potential-current (V - I) characteristics of the silica membrane from which we obtained the transference number, diffusion potential, and electrical resistance. In addition, we developed empirical correlations for the transference number and the area-specific resistance. Finally, we studied power generation by reverse electro dialysis using a silica membrane and developed a contour map of the power output density as a function of concentrations on the basis of the empirical correlations.

2. Materials and Methods

For the experiment, we used a porous alumina substrate (Anodisc 47, Whatman Inc., Marlborough, MA, USA), 47 mm in diameter and 60 μm thick. Figure 2 shows the scanning electron microscope (SEM) images of the top and cross section of the alumina substrate that had a nominal pore radius of 100 nm and a nominal pore density of $1.2 \times 10^9 \text{ cm}^{-2}$. An undoped 1 μm thick silica layer was deposited on the substrate by plasma-enhanced chemical vapor deposition (LAPECVD, Plasma-Therm, Saint Petersburg, FL, USA) at a deposition rate of 10.2 $\text{\AA}/\text{s}$ and 150 $^\circ\text{C}$, with SiH_4 , He, and N_2O as the processing gases. The silica layer was deposited on the front side of the substrate only. Figure 3 shows the SEM images of the top and cross section of the smooth and dense fabricated silica layer on top of the porous alumina substrate. In Figure 3, the alumina substrate has a nominal pore radius of 100 nm. As shown in Figure 3a, a well-defined pore structure is not observed in the top view of the silica layer. Therefore, we can conclude that this layer is a dense silica membrane. The fabricated silica membrane was placed at the center of a two-cell apparatus, a schematic diagram of which is shown in Figure 4 [22,23]. Two Ag/AgCl reference electrodes were fabricated by first coating silver mesh (05-1806-02, 40935, Nilaco Corp., Tokyo, Japan) with Ag/AgCl ink (011464, ALS Co. Ltd., Tokyo, Japan), washing the electrodes sufficiently with water, and leaving them overnight to dry. After placing the electrodes in the two cells, 0.5 L of a concentrated NaCl solution was placed into the desalting cell and 0.5 L of a dilute NaCl solution was placed into the concentrating cell. The pH of each solution was 5.4 ± 0.2 .

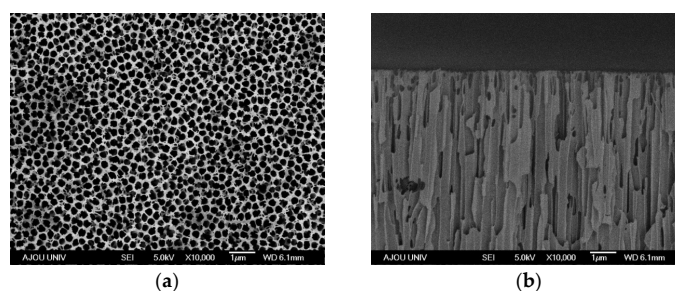


Figure 2. Scanning Electron Microscope (SEM) photos of the porous alumina substrate: (a) top view and (b) cross-sectional view.

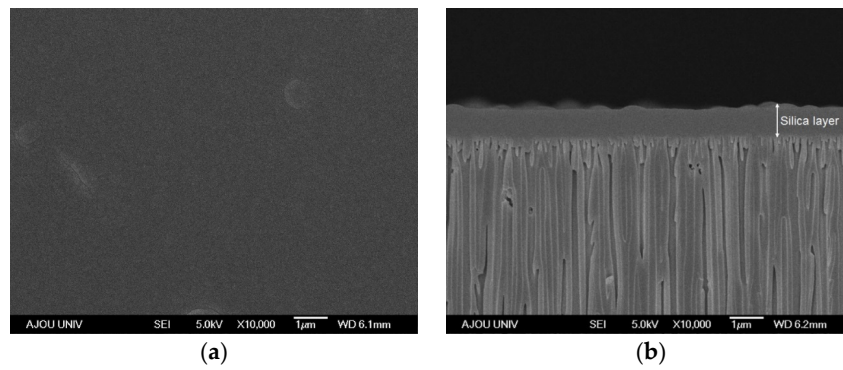


Figure 3. SEM photos of the silica layer on the porous alumina substrate: (a) top view and (b) cross-sectional view.

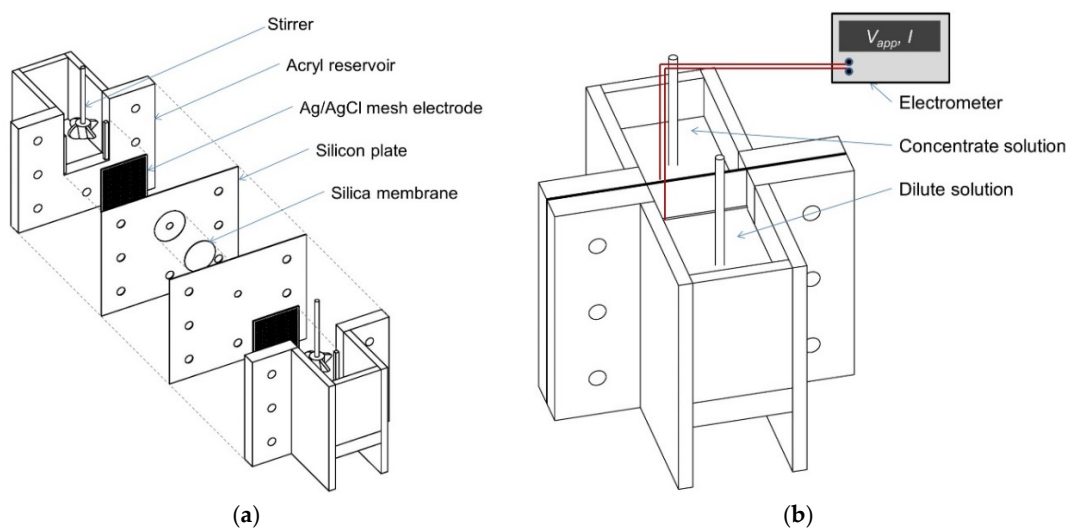


Figure 4. Experimental setup: (a) enlarged schematic and (b) normal schematic.

An electrometer (2410 Source Meter, Keithley Instruments Inc., Solon, OH, USA) recorded the current (I) from the silica layer for various applied voltages (V_{app}). The current was measured for 2 min in the steady state, *i.e.*, when the change in the current was less than $\pm 1\%$. The V - I characteristics were measured for various combinations of the concentrations of the dilute solution (c_L) and the concentrated solution (c_H), as listed in Table 1. We performed each experiment four times.

Table 1. Transference number, diffusion potential, area-specific resistance, and maximum power density for various combinations of NaCl concentrations.

c_L (M)	c_H (M)	t_+	E_{diff} (mV)	RA ($\Omega \cdot \text{cm}^2$)	P_{max}/A (mW/m ²)
0.0001	0.001	0.749 ± 0.001	29.2 ± 0.1	$14,600 \pm 100$	0.145 ± 0.00001
0.0001	0.01	0.736 ± 0.001	54.7 ± 0.1	$12,200 \pm 100$	0.611 ± 0.00001
0.0001	0.1	0.565 ± 0.001	22.2 ± 0.2	$10,500 \pm 100$	0.117 ± 0.00001
0.0001	1	0.424 ± 0.001	-34.1 ± 0.3	8100 ± 30	0.358 ± 0.00003
0.001	0.01	0.782 ± 0.004	32.4 ± 0.5	3300 ± 10	0.796 ± 0.00019
0.001	0.1	0.593 ± 0.001	20.9 ± 0.2	2250 ± 10	0.482 ± 0.00003
0.001	1	0.439 ± 0.004	-20.2 ± 1.3	2140 ± 10	0.477 ± 0.002
0.01	0.1	0.619 ± 0.003	13.2 ± 0.4	443 ± 2	0.976 ± 0.00074
0.01	1	0.461 ± 0.001	-8.3 ± 0.1	332 ± 3	0.521 ± 0.00002
0.1	1	0.465 ± 0.006	-3.7 ± 0.6	57.6 ± 0.2	0.591 ± 0.01796

3. Results and Discussion

The setup for this experiment can be represented in terms of basic circuit elements, as shown in Figure 5a. E_{redox} , E_{diff} , and R are the potential generated from redox reactions on the electrodes, the diffusion potential of the silica membrane, and the electric resistance of the silica membrane, respectively. The electric potential generated in the silica membrane, V , is defined as:

$$V = V_{\text{app}} - E_{\text{redox}} = E_{\text{diff}} - IR \quad (1)$$

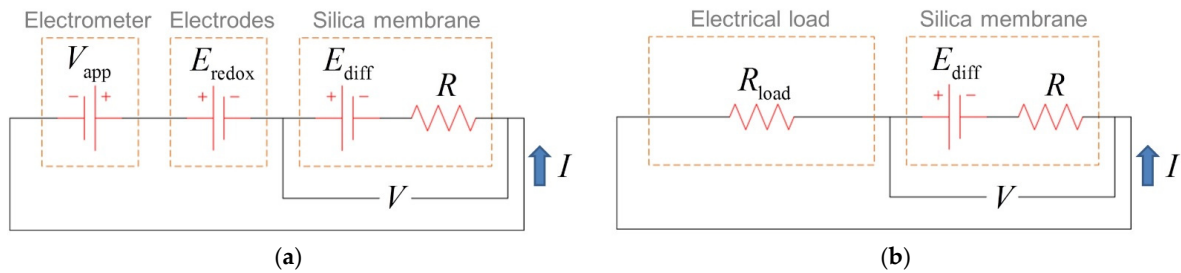


Figure 5. (a) Basic circuit elements representing the experimental setup; and (b) equivalent circuit for this setup in which the source meter and the electrode are considered the electrical load R_{load} connected to the silica membrane.

E_{redox} is produced by an unequal voltage drop at the electrode–solution interface in different electrolyte concentrations. The thermodynamic value of E_{redox} is defined as [21,24]:

$$E_{\text{redox}} = \frac{RT}{zF} \ln \frac{\gamma_{\text{C}_\text{H}} c_{\text{H}}}{\gamma_{\text{C}_\text{L}} c_{\text{L}}} \quad (2)$$

where R , T , z , F , and γ are the gas constant, temperature, charge number, Faraday constant, and mean activity coefficient, respectively. Another equivalent circuit for this setup is shown in Figure 5b, in which the source meter and the electrode are considered the electrical load R_{load} connected to the silica membrane. R_{load} is defined as:

$$R_{\text{load}} = \frac{V_{\text{app}} - E_{\text{redox}}}{I} = \frac{V}{I} \quad (3)$$

E_{redox} here is for the given concentrations of solutions. Therefore, by changing V_{app} , we can change the R_{load} connected to the silica membrane.

Figure 6a shows a typical potential-current (V - I) curve for the silica membrane. The electrical resistance R of the silica membrane is calculated using the slope of the curve. The potential decreases linearly as the current increases, emphasizing the ohmic behavior of the silica layer in the conducting current. This behavior occurs because the concentration profile inside the silica layer is not highly dependent on the electrical potential and because there is no polarization effect at the surface of the silica layer under small electric fields [25,26]. The zero-current potential on the V - I curve is E_{diff} and is determined by the difference between the diffusion fluxes of the positive and negative ions caused by the ion-selective property of the silica layer. Thus, the cations diffuse more rapidly than the anions when the concentrated solution diffuses into the dilute solution through the silica layer because of the ion-selective transport property of the silica layer. This rapid diffusion of cations into the dilute solution makes it positively charged and leaves the concentrated solution negatively charged. Thus, a double layer of positive and negative charges develops between the two solutions. This results in a difference in potential between the two solutions, *i.e.*, E_{diff} , which is defined as:

$$E_{\text{diff}} = (2t_+ - 1) \frac{RT}{zF} \ln \frac{\gamma_{\text{C}_\text{H}} c_{\text{H}}}{\gamma_{\text{C}_\text{L}} c_{\text{L}}} \quad (4)$$

where t_+ is the transference number for the cations and is defined as the fraction of the electrical current carried by the cations under an applied voltage. It is an index of the ion selectivity of the silica membrane: $t_+ = 1$ for complete cation selectivity, $t_+ = 0$ for complete anion selectivity, and $t_+ \approx 0.4$ for NaCl solutions when the membrane is not ion-selective [27]. In Figure 6a, E_{diff} is positive, *i.e.*, the silica membrane is cation-selective. Figure 6b shows a typical P - R_{load} curve of the silica layer. The generated power P is defined as:

$$P = VI \quad (5)$$

Combining Equations (1), (3) and (5) yields:

$$P = E_{\text{diff}}^2 \frac{R_{\text{load}}}{(R_{\text{load}} + R)^2} \quad (6)$$

Maximum power is generated when $R_{\text{load}} = R$; thus:

$$P_{\text{max}} = \frac{E_{\text{diff}}^2}{4R} \quad (7)$$

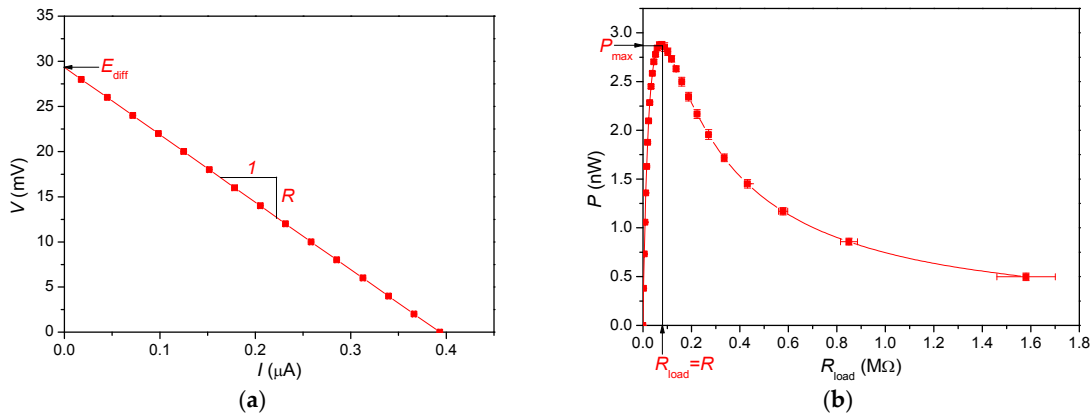


Figure 6. (a) V - I curve and (b) power generation *vs.* R_{load} for the silica membrane; $c_L = 0.1$ mM and $c_H = 1$ Mm.

We measured the I - V curves for various c_L and c_H and used them to calculate t_+ , R , E_{diff} , and P_{max} of the silica membrane for those concentrations. The results are presented in Figures 7–10 respectively, and each characteristic determined by the experimental results is discussed below:

(1) Figure 7 shows that t_+ strongly depends on c_H for various c_L . At the high-concentration limit ($c_H \approx 1$), t_+ is almost equal to that of the bulk solution ($t_+ \approx 0.4$). As c_H decreases, t_+ increases because the effect of the fixed anionic groups, which have an affinity for cations, increases as their density increases compared to the bulk ion concentration [28,29]. From the experimental data, we obtained an empirical correlation for t_+ using a least-squares fit:

$$t_+ = 0.495 - 0.0715 \ln c_H + 0.00873 \ln c_L \quad (8)$$

Figure 7 also shows t_+ calculated using Equation (8). The calculated values agree well with the experimental data when c_H and c_L are >10 mM.

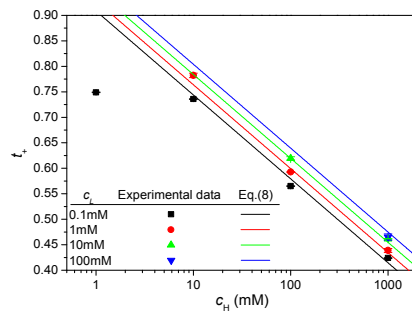


Figure 7. Transference number for various concentrations of both NaCl solutions.

(2) Figure 8 presents E_{diff} as a function of c_H and c_L . Figure 8 shows that E_{diff} is maximized at a particular concentration of the concentrated solution (c_H). This effect is seen in Equation (4) where $\ln(\gamma_{c_H}c_H/\gamma_{c_L}c_L)$ increases as c_H increases while $2t_+ - 1$ decreases. Figure 8 also shows E_{diff} calculated using Equations (4) and (8) and that those values match the experimental data well when c_H and c_L are >10 mM.

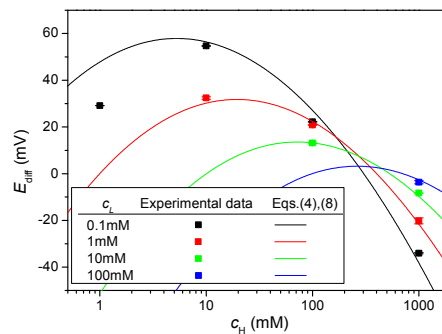


Figure 8. Open circuit voltage for various concentrations of both NaCl solutions.

(3) Figure 9 presents the resistance per unit cross-sectional area multiplied by the total cross-sectional area of the membrane, RA , as a function of c_H for various c_L . As c_H and c_L increase, the bulk concentration of ions in the silica layer increases, which causes R to decrease. R has a strong dependence on c_L and a weak dependence on c_H . We obtained an empirical correlation for RA by fitting the experimental data to the following equation:

$$RA = 0.00134c_H^{-0.0891}c_L^{-0.705} \tag{9}$$

Figure 9 also shows RA calculated using Equation (9) and that the results agree well with the experimental data.

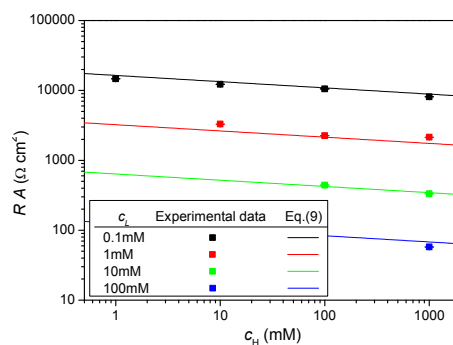


Figure 9. Area-specific resistance for various concentrations of both NaCl solutions.

(4) Figure 10 shows the maximum power output per unit cross-sectional area, P_{\max}/A , as a function of c_H for various c_L . The highest P_{\max}/A measured was 0.98 mW/m^2 when $c_L = 0.1 \text{ mM}$ and $c_H = 10 \text{ mM}$. By combining Equations (4) and (7), P_{\max} is expressed as:

$$P_{\max} = \frac{(2t_+ - 1)^2}{4R} \left(\frac{RT}{zF} \right)^2 \left(\ln \frac{\gamma_{C_H} c_H}{\gamma_{C_L} c_L} \right)^2 \quad (10)$$

Figure 10 also shows P_{\max}/A calculated using Equations (8)–(10) and that the values agree well with the experimental data. Power is generated at low concentrations because of the cation selectivity of the silica membrane. At high concentrations ($c_H = 1 \text{ M}$), ion selectivity of the silica membrane is almost nonexistent, as shown in Figure 7. However, even in this case, a small amount of power can be generated from the natural anion selectivity of bulk NaCl solutions ($t_+ \approx 0.4$). Finally, Figure 11 shows the contour plots of P_{\max}/A , calculated using Equations (8)–(10), as a function of c_L and c_H . The figure shows that the optimal concentrations at which the power output density is maximum (1.2 mW/m^2) are $c_L = 4 \text{ mM}$ and $c_H = 50 \text{ mM}$. That maximum P_{\max}/A value corresponds to a power output of $2.1 \text{ } \mu\text{W}$ because the cross-sectional area of the membrane, A , used in the present study was 17.3 cm^2 . This power output is sufficient to drive low-power circuitry for wireless systems and to power biomedical implant devices [30,31]. Therefore, dense silica membranes have the potential for use in nanofluidic and microfluidic systems.

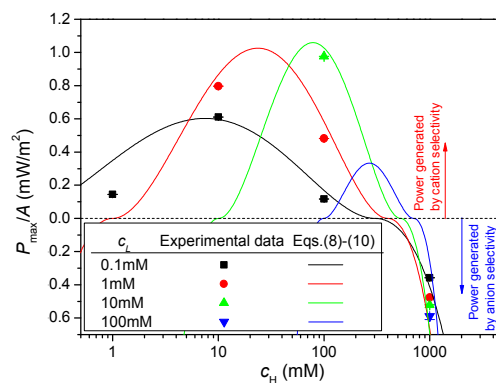


Figure 10. Maximum power generation density for various concentrations of both NaCl solutions.

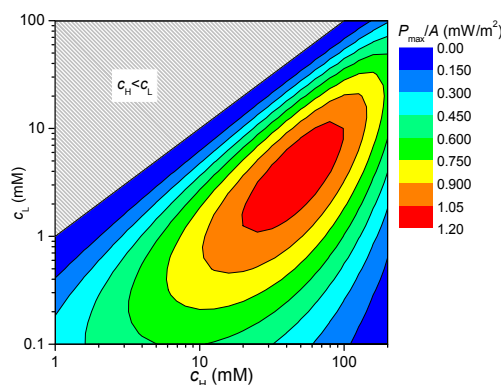


Figure 11. Contour map of maximum power generation density as a function of c_L and c_H .

(5) Figure 12 shows the energy conversion efficiency corresponding to the maximum power generation for various c_H and c_L values. As given in Reference [32], energy conversion efficiency is

defined as the ratio of the output energy (electrical energy) to the input energy (Gibbs free energy of mixing) [14], as shown in Equation (11):

$$\eta = \frac{VI}{RT \left(\ln \frac{\gamma_{\text{CH}} c_{\text{H}}}{\gamma_{\text{CL}} c_{\text{L}}} \right) (J_{+} + J_{-})} \quad (11)$$

Here, J_{+} and J_{-} are cation flux and anion flux through the membrane, respectively. The motion of cations and anions through the membrane gives rise to a current. The current is expressed by Equation (12):

$$I = zF(J_{+} - J_{-}) \quad (12)$$

The transference number for the cations is defined as the fraction of the electrical current carried by the cations under an applied voltage, according to Equation (13):

$$t_{+} \approx \frac{zFJ_{+}}{I} = \frac{J_{+}}{J_{+} - J_{-}} \quad (13)$$

In Figure 6b, we can see that the maximum power is generated when $R_{\text{load}} = R$. From Equations (1) and (3), and $R_{\text{load}} = R$, the voltage corresponding to the maximum power generation satisfies Equation (14):

$$V = \frac{E_{\text{diff}}}{2} \quad (14)$$

Finally, by combining Equations (2) and (11)–(14), we obtain Equation (15), a formula for the energy conversion efficiency corresponding to the maximum power generation:

$$\eta = \frac{(2t_{+} - 1)^2}{2} \quad (15)$$

This equation was also used for calculating the efficiency in references [15,18]. As shown in Figure 12 and Equation (15), the highest efficiency is achieved when the transference number is the greatest. The best efficiency obtained in the present study is 16%.

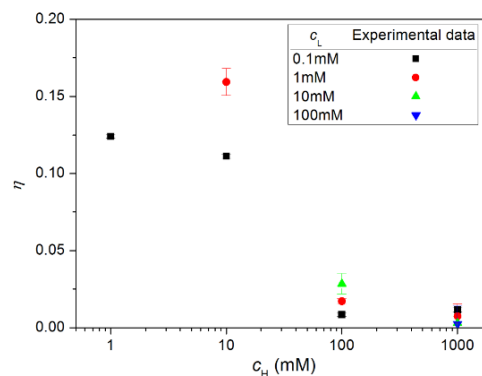


Figure 12. Energy conversion efficiency for various concentrations of NaCl solutions.

4. Conclusions

We investigated power generation by reverse electro dialysis in a dense silica membrane that was between two NaCl solutions with various combinations of concentrations. The highest measured power output density was 0.98 mW/m^2 . In addition, the power output density was calculated on the basis of empirical correlations for the transference number and the area-specific electrical resistance. The contour map of the power output density as a function of the concentrations of the NaCl solutions showed that a power output density of 1.2 mW/m^2 is possible, a level that is sufficient to drive

nanofluidic and microfluidic systems. Therefore, dense silica membranes have the potential for use as micro power generators in nanofluidic and microfluidic systems.

Acknowledgments: This research was supported by the Nano Material Technology Development Program through the National Research Foundation of Korea (NRF), funded by the Ministry of Science, ICT and Future Planning (NRF-2011-0030285).

Author Contributions: Sang Woo Lee and Dong-Kwon Kim conceived and designed the experiments; Sang Woo Lee performed the experiments; Hyun Jung Kim and Dong-Kwon Kim analyzed the data; Dong-Kwon Kim wrote the paper.

Conflicts of Interest: The authors declare no conflict of interest.

References

1. White, B.E. Energy-harvesting devices: Beyond the battery. *Nat. Nanotechnol.* **2008**, *3*, 71–72. [[CrossRef](#)] [[PubMed](#)]
2. Pennathur, S.; Eijkel, J.C.T.; Van Den Berg, A. Energy conversion in microsystems: Is there a role for micro/nanofluidics? *Lab Chip* **2007**, *7*, 1234–1237. [[PubMed](#)]
3. Majumdar, A.; Tien, C.L. Micro power devices. *Microscale Thermophys. Eng.* **1998**, *2*, 67–69.
4. Whalen, S.; Thompson, M.; Bahr, D.; Richards, C.; Richards, R. Design, fabrication and testing of the P 3 micro heat engine. *Sens. Actuators A Phys.* **2003**, *104*, 290–298. [[CrossRef](#)]
5. Choban, E.R.; Markoski, L.J.; Wieckowski, A.; Kenis, P.J. Microfluidic fuel cell based on laminar flow. *J. Power Sources* **2004**, *128*, 54–60. [[CrossRef](#)]
6. Van Der Heyden, F.H.; Bonthuis, D.J.; Stein, D.; Meyer, C.; Dekker, C. Power generation by pressure-driven transport of ions in nanofluidic channels. *Nano Lett.* **2007**, *7*, 1022–1025. [[CrossRef](#)] [[PubMed](#)]
7. Tanaka, Y.; Sato, K.; Shimizu, T.; Yamato, M.; Okano, T.; Kitamori, T. A micro-spherical heart pump powered by cultured cardiomyocytes. *Lab Chip* **2007**, *7*, 207–212. [[CrossRef](#)] [[PubMed](#)]
8. Chang, C.C.; Yang, R.J. Electrokinetic energy conversion efficiency in ion-selective nanopores. *Appl. Phys. Lett.* **2011**, *99*, 083102. [[CrossRef](#)]
9. Chang, C.C.; Yang, R.J. Electrokinetic energy conversion in micrometer-length nanofluidic channels. *Microfluid. Nanofluid.* **2010**, *9*, 225–241. [[CrossRef](#)]
10. Hsieh, H.P. *Inorganic Membranes for Separation and Reaction*; Elsevier: Amsterdam, The Netherlands, 1996.
11. Hunter, R.J. *Zeta Potential in Colloid Science*; Academic Press: London, UK, 1981.
12. Baucke, F.G.K. The modern understanding of the glass electrode response. *Fresenius' J. Anal. Chem.* **1994**, *349*, 582–596. [[CrossRef](#)]
13. Eisenman, G. Cation selective glass electrodes and their mode of operation. *Biophys. J.* **1962**, *2*, 259–323. [[CrossRef](#)]
14. Bocquet, L.; Charlaix, E. Nanofluidics, from bulk to interfaces. *Chem. Soc. Rev.* **2010**, *39*, 1073–1095. [[CrossRef](#)] [[PubMed](#)]
15. Kim, D.K.; Duan, C.; Chen, Y.F.; Majumdar, A. Power generation from concentration gradient by reverse electro dialysis in ion-selective nanochannels. *Microfluid. Nanofluid.* **2010**, *9*, 1215–1224. [[CrossRef](#)]
16. Ouyang, W.; Wang, W.; Zhang, H.; Wu, W.; Li, Z. Nanofluidic crystal: A facile, high-efficiency and high-power-density scaling up scheme for energy harvesting based on nanofluidic reverse electro dialysis. *Nanotechnology* **2013**, *24*. [[CrossRef](#)] [[PubMed](#)]
17. Kim, J.; Kim, S.J.; Kim, D.K. Energy harvesting from salinity gradient by reverse electro dialysis with anodic alumina nanopores. *Energy* **2013**, *51*, 413–421. [[CrossRef](#)]
18. Yeh, H.C.; Chang, C.C.; Yang, R.J. Reverse electro dialysis in conical-shaped nanopores: Salinity gradient-driven power generation. *RSC Adv.* **2014**, *4*, 2705–2714. [[CrossRef](#)]
19. Chu, K.L.; Shannon, M.A.; Masel, R.I. An improved miniature direct formic acid fuel cell based on nanoporous silicon for portable power generation. *J. Electrochem. Soc.* **2006**, *153*, A1562–A1567. [[CrossRef](#)]
20. Lee, S.; Park, M.; Park, H.S.; Kim, Y.; Cho, S.; Cho, J.H.; Park, J.; Hwang, W. A polyethylene oxide-functionalized self-organized alumina nanochannel array for an immunoprotection biofilter. *Lab Chip* **2011**, *11*, 1049–1053. [[CrossRef](#)] [[PubMed](#)]
21. Bard, A.J.; Faulkner, L.R. *Electrochemical Methods*; John Wiley & Sons: New York, NY, USA, 2001.

22. Tanaka, Y. *Ion Exchange Membranes: Fundamentals and Applications*; Elsevier Science & Technology: Amsterdam, The Netherlands, 2007.
23. Kang, B.D.; Kim, H.J.; Lee, M.G.; Kim, D.K. Numerical study on energy harvesting from concentration gradient by reverse electrodialysis in anodic alumina nanopores. *Energy* **2015**, *86*, 525–538. [[CrossRef](#)]
24. Lakshminarayanaiah, N. *Transport Phenomena in Membranes*; Academic Press: New York, NY, USA, 1969.
25. Kim, S.J.; Wang, Y.C.; Lee, J.H.; Jang, H.; Han, J. Concentration polarization and nonlinear electrokinetic flow near a nanofluidic channel. *Phys. Rev. Lett.* **2007**, *99*. [[CrossRef](#)] [[PubMed](#)]
26. Vlassiouk, I.; Smirnov, S.; Siwy, Z. Ionic selectivity of single nanochannels. *Nano Lett.* **2008**, *8*, 1978–1985. [[CrossRef](#)] [[PubMed](#)]
27. Fry, C.H.; Langley, S.E.M. *Ion-Selective Electrodes for Biological Systems*; Chemical Rubber Company (CRC) Press: Boca Raton, FL, USA, 2002.
28. Karnik, R.; Castelino, K.; Fan, R.; Yang, P.; Majumdar, A. Effects of biological reactions and modifications on conductance of nanofluidic channels. *Nano Lett.* **2005**, *5*, 1638–1642. [[CrossRef](#)] [[PubMed](#)]
29. Stein, D.; Kruithof, M.; Dekker, C. Surface-charge-governed ion transport in nanofluidic channels. *Phys. Rev. Lett.* **2004**, *93*. [[CrossRef](#)] [[PubMed](#)]
30. Najafi, K.; Galchev, T.; Aktakka, E.E.; Peterson, R.L.; McCullagh, J. Microsystems for Energy Harvesting. In Proceedings of the 2011 16th International Solid-State Sensors, Actuators and Microsystems Conference (TRANSDUCERS), Beijing, China, 5–9 June 2011; pp. 1845–1850.
31. Wang, Z.L. Self-powered nanotech. *Sci. Am.* **2008**, *298*, 82–87. [[CrossRef](#)] [[PubMed](#)]
32. Fair, J.C.; Osterle, J.F. Reverse electrodialysis in charged capillary membranes. *J. Chem. Phys.* **1971**, *54*, 3307–3316. [[CrossRef](#)]



© 2016 by the authors; licensee MDPI, Basel, Switzerland. This article is an open access article distributed under the terms and conditions of the Creative Commons by Attribution (CC-BY) license (<http://creativecommons.org/licenses/by/4.0/>).